Completion of Oil Wells

John Rudge

May 4, 2003

1 Introduction

After the initial drilling of an oil well, a circular steel pipe is lowered into the hole and cement is pumped up through the thin eccentric annulus between the steel pipe and the drilled rock. This cement drives out mud that initially fills the thin annulus. Due to the eccentricity of the annulus, the flow of cement is faster on the wider side of the annulus leading to the possibility of channelling of cement through the mud, leaving a layer of mud behind on the narrow side. However, the cement is usually more dense than the mud and this causes an azimuthal flow of the denser cement toward the narrow side reducing this channelling effect. As such, under some circumstances it is thought that stable steady state displacements can occur. This project sets out to investigate this flow.

2 Approach

A highly idealised version of this problem is examined. The radius a of the steel pipe is large compared to the narrow gap $h(\theta)$ between the pipe and the rock. The length of the pipe $2L$ is also large compared to this thin gap. The cement and mud are treated as Newtonian viscous fluids. Given the small gap, lubrication theory can be used to study the flow.

Non-dimensionalise all lengths on the gap thickness. Let $h(\theta) = 1 + \epsilon \cos\theta$, where ϵ gives the eccentricity of the annulus.

Introduce the dynamic pressure $p_{dyn} = p - \rho g z$. Henceforth drop the dyn suffix and work with dynamic pressure. The thin layer approximations give

$$\mu \frac{\partial^2 u_\theta}{\partial r^2} = \frac{1}{a}\frac{\partial p}{\partial \theta}$$

$$\mu \frac{\partial^2 u_z}{\partial r^2} = \frac{\partial p}{\partial z}$$

Here cylindrical polar co-ordinates centred at the centre of the pipe are used. r is taken to be the distance away from the inner pipe. Assume μ, ρ are constant for given θ, z; i.e. ignore radial variation. Under this assumption these equations can be easily integrated up to find the velocity field.

$$u_\theta = \frac{1}{2\mu a}\frac{\partial p}{\partial \theta} r(r-h)$$

$$u_z = \frac{1}{2\mu}\frac{\partial p}{\partial z} r(r-h)$$

Integrating this over the gap yields the volume flux which can be concisely written as:

$$\mathbf{q} = \frac{h^3}{12\mu}\nabla p$$

Conservation of volume flux gives simply $\nabla.\mathbf{q} = 0$. Note that μ may be discontinuous across the boundary. Across the interface there is continuity of tangential velocity; $\mathbf{u}.\mathbf{n}$ is continuous. This implies $\mathbf{q}.\mathbf{n}$ is continuous across the boundary. Pressure must also be continuous across the interface, and hence there is a jump in the dynamic pressure across interface given by $[p]_{\text{interface}} = -[\rho]_{\text{interface}} gz$.

Let the cement have viscosity μ_1, density ρ_1, and let the applied dynamic pressure gradient at $z = -L$ be G_1. Similarly the parameters for the mud are μ_2, ρ_2, and the applied gradient at $z = L$ is G_2. Note conservation of flux in and out the pipe imposes:

$$\frac{G_1}{\mu_1} = \frac{G_2}{\mu_2}$$

We can further non-dimensionalise the problem by scaling viscosities with μ_1 and pressures with G_1. Hence the important non-dimensional parameters in this problem are:

$$\tilde{\mu} = \frac{\mu_2}{\mu_1} \text{ and } \tilde{\rho} = \frac{(\rho_1 - \rho_2)g}{G_1}$$

along with non-dimensional lengths a, L, and the eccentricity parameter ϵ.

To track the interface introduce a level set function $\phi(\theta, z, t)$. This is a continuous function, the zero level set of which gives the location of the interface. Usually a signed distance function is used. $\phi < 0$ in the cement, and $\phi \geq 0$ for the mud. The level set equation governing the motion of the interface is [5]:

$$\frac{\partial \phi}{\partial t} + \bar{\mathbf{u}}.\nabla\phi = 0$$

Here $\bar{\mathbf{u}}$ is the averaged velocity over r given by

$$\bar{\mathbf{u}} = \frac{\mathbf{q}}{h}$$

An example initial starting condition would be a flat interface given by a level set function $\phi(\theta, z, 0) = z$.

Therefore, the problem breaks down into solving a hyperbolic system for the level set function, within which an elliptic problem is solved for the velocity field at each time step.

3 Elliptic Problem

In solving this problem numerically the following elliptic problem, a modified Poisson equation, has to be tackled:

$$\nabla.\left(\frac{h^3}{\mu}\nabla p\right) = 0$$

Subject to boundary conditions on the interface

$$[p]_{\text{interface}} = -[\rho]_{\text{interface}} gz$$

$$\left[\frac{h^3}{\mu}\nabla p.\mathbf{n}\right]_{\text{interface}} = 0$$

and Neumann boundary conditions at the ends

$$\frac{dp}{dz} = G_1 \text{ on } z = -L$$

$$\frac{dp}{dz} = G_2 \text{ on } z = L$$

To solve this the method of Liu, Fedkiw, and Kang [3] was used. This method has the advantage of being easy to implement and can be easily solved with "black box" solvers built into Matlab. The resultant matrix problem is sparse symmetric positive definite, and was solved using preconditioned conjugate gradients with an incomplete Cholesky pre-conditioner (using Matlab's pcg and cholinc functions) as recommended in [2]. Since this is an iterative scheme the solution at the previous time step can be exploited to speed up the calculations. In practise very few iterations of pcg were needed at each time step. The main disadvantage of this method is that it is first order, which can cause problems as it is the velocity field, not the pressure field that we are most interested in. However, second order methods are harder to implement, produce harder to solve asymmetric systems, and so for this project this method was used.

Following the notation of Liu et al. have a variable coefficient Poisson equation of the form:

$$\nabla.(\beta(\theta, z)\nabla p) = 0$$

$$[p]_{\text{interface}} = a(\theta, z) = (\rho_1 - \rho_2)gz$$

$$[\beta\nabla p.\mathbf{n}]_{\text{interface}} = b(\theta, z) = 0$$

Where

$$\beta(\theta, z) = \frac{h^3(\theta)}{\mu(\theta, z)}$$

Set up a grid of n points in θ, and m points in z. Introduce variables $p_{i,j}$, $\beta_{i,j}$, and $a_{i,j}$ (corresponding to $p(\theta, z)$, $\beta(\theta, z)$, and $a(\theta, z)$ respectively) at each grid point. To avoid introducing unnecessary anisotropy in the elliptic solver n and m were always chosen so that $a\Delta\theta = \Delta z$.

The governing equation becomes:

$$\frac{\beta_{i+\frac{1}{2},j}\left(\frac{p_{i+1,j}-p_{i,j}}{a\Delta\theta}\right) - \beta_{i-\frac{1}{2},j}\left(\frac{p_{i,j}-p_{i-1,j}}{a\Delta\theta}\right)}{a\Delta\theta} + \frac{\beta_{i,j+\frac{1}{2}}\left(\frac{p_{i,j+1}-p_{i,j}}{\Delta z}\right) - \beta_{i,j-\frac{1}{2}}\left(\frac{p_{i,j}-p_{i,j-1}}{\Delta z}\right)}{\Delta z} = g_{i,j} + F^{\theta}_{i,j} + F^{z}_{i,j}$$

Where $g_{i,j}$ is a term from the boundary condition at the ends, and $F^{\theta}_{i,j}$ and $F^{z}_{i,j}$ are terms from the boundary condition across the interface.

Each $\beta_{i-\frac{1}{2},j}$ is calculated from the side of the interface that $x_{i-1,j}$ and $x_{i,j}$ lie on. If they both lie on the same side then β at the midpoint can be calculated directly from the formula. Otherwise interpolate as follows.

$$\beta_{i-\frac{1}{2},j} = \frac{\beta_{i-1,j}\beta_{i,j}\left(|\phi_{i-1,j}| + |\phi_{i,j}|\right)}{\beta_{i,j}|\phi_{i-1,j}| + \beta_{i-1,j}|\phi_{i,j}|}$$

Similarly $\beta_{i,j-\frac{1}{2}}$ can be defined.

Let $F^\theta = F^L + F^R$ and $F^z = F^B + F^T$. Consider the left arm of the stencil connecting $x_{i,j}$ and $x_{i-1,j}$. If both points lie on the same side of the interface let $F^L_{i,j}$=0. Otherwise let

$$a_\Gamma = \frac{a_{i,j}|\phi_{i-1,j}| + a_{i-1,j}|\phi_{i,j}|}{|\phi_{i,j}| + |\phi_{i-1,j}|}$$

If $\phi_{i,j} < 0$ and $\phi_{i-1,j} \geq 0$, then

$$F^L_{i,j} = \frac{\beta_{i-\frac{1}{2},j} a_\Gamma}{(a\Delta\theta)^2}$$

Otherwise

$$F^L_{i,j} = -\frac{\beta_{i-\frac{1}{2},j} a_\Gamma}{(a\Delta\theta)^2}$$

Similarly we can define F for the other arms of the stencil.

Neumann boundary conditions at the end of the pipe give $g_{i,j}$ non zero only for the following values:

$$g_{i,1} = \frac{\beta_{i,\frac{1}{2}} G_1}{\Delta z}$$

$$g_{i,m} = -\frac{\beta_{i,m+\frac{1}{2}} G_2}{\Delta z}$$

Periodic boundary conditions are easily applied by letting $x_{n+1,j} = x_{1,j}$ for example.

4 Hyperbolic problem

The hyperbolic equation to solve is

$$\frac{\partial \phi}{\partial t} + \mathbf{u}.\nabla\phi = 0$$

To tackle this an adaption of the methods of Sussman, Fatemi, Smereka and Osher [6] were used. The method for solving the elliptic problem gives the velocity field on the edges of the main grid - i.e. have $u^\theta_{i-\frac{1}{2},j}$ and $u^z_{i,j-\frac{1}{2}}$, where these are calculated in the same way as the gradient of p is in the discretisation of the Poisson problem, taking in to account the discontinuity factors $g_{i,j}$ and $F_{i,j}$. Simple averaging is then used to get the values on the main grid.

$$u^\theta_{i,j} = \frac{u^\theta_{i+\frac{1}{2},j} + u^\theta_{i-\frac{1}{2},j}}{2}$$

$$u^z_{i,j} = \frac{u^z_{i,j+\frac{1}{2}} + u^z_{i,j-\frac{1}{2}}}{2}$$

The $\mathbf{u}.\nabla\phi$ term is then disretised as follows:

$$\mathbf{u}.\nabla\phi = \frac{u^\theta_{i,j}\left(\phi_{i+\frac{1}{2},j} - \phi_{i-\frac{1}{2},j}\right)}{a\Delta\theta} + \frac{u^z_{i,j}\left(\phi_{i,j+\frac{1}{2}} - \phi_{i,j-\frac{1}{2}}\right)}{\Delta z}$$

Where the edge values of ϕ are calculated from the following first order up-winding scheme:

$$k_1 = \begin{cases} i-1 & u^{\theta}_{i-\frac{1}{2},j} \geq 0 \\ i & \text{otherwise} \end{cases}$$

$$\phi_{i-\frac{1}{2},j} = \phi_{k_1,j}$$

$\phi_{i,j-\frac{1}{2}}$ is calculated similarly.
The temporal derivative is discretised using a simple Euler scheme.

$$\phi^{k+1} = \phi^k - \Delta t(\mathbf{u}.\nabla\phi)^k$$

Finally, there is a CFL time step restriction given by:

$$\Delta t \left(\frac{|u^{\theta}|_{\max}}{a\Delta\theta} + \frac{|u^z|_{\max}}{\Delta z} \right) \leq \frac{1}{2}$$

There are many more sophisticated methods for solving this hyperbolic system, but for reasons of speed of development this simple scheme was used. Simple refinements include Runge-Kutta schemes which can easily extend the Euler update to higher accuracy. Higher order up-winding schemes are also available.

5 Testing the elliptic solver

Simple checks of the elliptic solver were made. The matrix system was confirmed to be positive definite, symmetric, and the existence of a zero eigenvalue with eigenvector of ones was confirmed (this exists since pressure is unique up to a constant). Figures 1 and 2 show the change in the calculated velocity by the elliptic solver under some given example parameters. A large sinusoidal interface has been chosen in both cases. The example data used had viscosity ratio $\tilde{\mu} = 2$, density difference $\tilde{\rho} = 2$, eccentricity $\epsilon = 0.5$, radius $a = 100$, and length $L = 100$. In figure 1 u_z is calculated at a position away from the interface. The graph oscillates, but the oscillations do seem to get smaller as the step size is reduced, and it seems possible that u_z is converging at this point, although it is hard to say at what order. Note that there are at least three figures of accuracy for all step sizes chosen.

Figure 2 shows the velocity as calculated at a point on the interface. Looking at the values for small step sizes a linear trend can be observed, demonstrating first order convergence. For step sizes less than 0.1 (around 60 mesh points in each direction) three significant figure accuracy starts be achieved.

Although the figures give some evidence for a first order convergence in the elliptic solver, it is not something to be expected from an analysis of the algorithm. The algorithm as it stands can be shown only to be first order in solving for the pressure, and as such we should not expect it to be first order in the velocity field which is essentially the derivative of the pressure field. However, due the additional complications in programming a second order algorithm, this solver was used.

6 Results

In runs of the program $a = 100$ was used throughout as an example of a large pipe radius compared to the gap thickness, and in most cases $L = 100\pi$. Larger L values were occasionally used when examining late time behaviour. The subsequent graphs show plots of the interface at set time intervals

so the motion of the interface can be seen. z is plotted against $a\theta$ with the lower fluid being the cement which is being pumped upwards against gravity into the mud.

There are a few simple tests of the full program that can be made. Figure 3 clearly demonstrates the convergence as the step size is reduced for some particular parameters. Note that the cement is more dense and more viscous than the mud in this example. Figure 4 shows the straightforward advection for the non-eccentric problem. This particular case can be solved easily analytically, and has a piecewise linear pressure profile. Analytically it can be shown that the non-dimensional mean velocity is $\bar{u} = \frac{1}{12}$. The program solves for this velocity exactly.

Eccentricity causing channelling can be seen in figure 5. Here there is no difference in viscosity or density between the two fluids, so they are essentially a single fluid. Only the eccentricity parameter is changed. Note that it seems that the velocity at the centre of the wide side of the annulus depends linearly on the eccentricity. Also, note that the velocity on the narrow side is very much reduced as the eccentricity increases, showing a stronger power law dependence.

Figure 6 shows the effect of a density difference on the flow in an eccentric annulus, with viscosity identical between the two fluids. With the cement denser than the mud a steady state appears to form and the azimuthal flow reduces the channelling effect. As the density difference grows the profile becomes flatter, as expected since this increases the azimuthal flow. The case of the mud being more dense than the cement has not be examined as it is unstable - in fact it is an example of a Rayleigh-Taylor instability, and the program is not able to resolve the detail needed to study this effect. However, this is the unphysical case as in practise the cement is always more dense than the mud.

Figure 7 looks at the steady state density difference problem more closely. Carrying on with the parameter values studied in figure 6 it shows a plot of the reciprocal of the steady state height against density difference. The steady state height was determined after a fixed time, a time chosen so that visually at least steady state seemed to be achieved. Note the clear linear trend, which suggests that the height is inversely proportional to the density parameter. The extrapolated linear best fit line does not quite go through the origin, but the predicted equilibrium height for zero density difference is around twice the length of the tube so is fairly large. There should not be a steady state when there is no difference in the properties of the two fluids, as the fluid on the wider side will always move faster than on the narrow side and there is no azimuthal flow. It is expected that greater numerical resolution will make the predicted equilibrium height at zero density difference even larger.

Figure 8 looks at the viscosity ratio when the cement is more viscous than the mud, all other parameters constant. As the cement is made more viscous the channelling effect is reduced, but unlike in the density case it doesn't seem to tend to a flat profile in the limit of zero viscosity ratio, and instead tends to a curved profile. Note the close similarity between the last three pictures. There doesn't seem to be any significant change in behaviour when reducing the viscosity ratio below $\tilde{\mu} = 0.1$. Figure 9 shows the case when the mud is more viscous. This increases the channelling effect, and an instability can be observed as the finger of cement gets longer. Again, note a close similarity between the last three pictures, and in this case there doesn't seem to be a significant change in behaviour when increasing the viscosity ratio above $\tilde{\mu} = 10$.

Figure 10 examines this instability further. It shows a particular example run with positive viscosity ratio for increasing step size. When the finger becomes steep oscillations occur on the interface. These oscillations have a frequency related to the the grid size, which suggests they may be numerical instabilities. Note the sharp gradient changes in the oscillations shown in the step pattern on the interface. However, before the oscillations set in there does seem to be good agreement in the interface position with step size.

7 Conclusions

This simple model shows a lot of the features that have been found in more complicated models and in experimental results. Bittleston, Ferguson and Frigaard [1] look at numerics for a more complicated non-Newtonian model and they also find steady state displacements and static channels on the narrow side under certain conditions. They do not use the method of level sets, and instead have a concentration variable which leads to a certain smearing of the interface which level set methods avoid. Curiously, they also mention the existence of an instability when the cement finger extends too far ahead, and they too have problems distinguishing between physical and numerical phenomena for this case. Pelipenko and Frigaard [4] have gone on to extend this work with a more analytic look at the problem and have proved the existence of steady state displacements in their model, which should be able to be adapted to this simpler model.

Experimental results [7] show that a positive density difference improves the displacement efficiency - as can be seen from this model, as it causes steady state displacements with decreasing equilibrium height. Also, for situations where the interface starts to become vertical interfacial instabilities were observed, which suggests the instabilities observed in the model may be a manifestation of true instabilities in the flow. Certainly it is important to investigate further the cause of the oscillations that were observed in figures 9 and 10.

Throughout this project there has been an emphasis on speed of development. As such in choice of methods simplicity has been the main deciding factor. Matlab was chosen for development for this reason, as although it may not produce the most optimised code it is easy to use built in routines for solving linear systems, graph plotting and the like. As such there is a lot of room for further optimisation of the method. Some better hyperbolic solvers should be investigated - there are good schemes for third order up-winding and third order Runge-Kutta methods which could be used [6]. This would allow a better study of the instabilities that have been observed to see if they are numerical or features of the flow. Improving the elliptic solver will probably prove harder. Second order methods such as the "immersed interface" method are thought to have a number of problems [3], and in particular have problems obtaining discontinuous solution profiles as is needed in this problem. A further improvement to the numerical algorithm would be by including a re-distancing routine, which would return the level-set function closer to a signed distance function at each step as used in [6]. This stops the level set function becoming too steep, but in practise this effect was not observed so this may be unnecessary.

Overall this method seems a good way of investigating the problem, and there are many ways it could be extended. Modern drilling methods produce more horizontal configurations [1] and this can be easily added in to the model by changing the jump condition on the pressure. Non-Newtonian effects could be considered, perhaps by applying the level sets methods to the model of Frigaard et al.[4], but it is probably best to understand the features of the Newtonian model further first. It would be good to examine the combined effects of density and viscosity, going beyond the single parameter variations discussed earlier. Since this model is fairly simple further analytic work should be able to be done, for example the steady shape profile for small eccentricity may be able to be calculated analytically in a similar way to Frigaard et al. [4] in their model. In particular it would be good to compare this with the main result found from these numerics, namely of the steady state height being inversely proportional to the density difference parameter.

References

[1] S.H Bittleson, J. Ferguson, and I.A. Frigaard. Mud removal and cement placement during primary cementing of an oil well. *J. Engineering Mathematics, to appear in special issue on industrial mathematics*, 2002.

[2] Myungjoo Kang, Ronald P. Fedkiw, and Xu-Dong Liu. A boundary condition capturing method for multiphase incompressible flow. *J. Sci. Comput.*, 15:323–360, 2000.

[3] Xu-Dong Liu, Ronald P. Fedkiw, and Myungjoo Kang. A boundary condition capturing method for poisson's equation on irregular domains. *J. Comput. Phys.*, 160:151–178, 2000.

[4] S. Pelipenko and I.A. Frigaard. On steady state displacements in primary cementing of an oil well. *Submitted to Journal of Engineering Mathematics*, 2002.

[5] J.A. Sethian. *Level Set Methods and Fast Marching Methods*. Cambridge University Press, second edition, 1999.

[6] Mark Sussman, Emad Fatemi, Peter Smereka, and Stanley Osher. An improved level set method for incompressible two-phase flows. *Computers and Fluids*, 27(5-6):663–680, 1998.

[7] M.A. Tehrani, S.H. Bittleston, and P.J.G. Long. Flow instabilities during annular displacement of one non-newtonian fluid by another. In *Experiments in Fluids*, volume 14. Springer-Verlag, 1993.

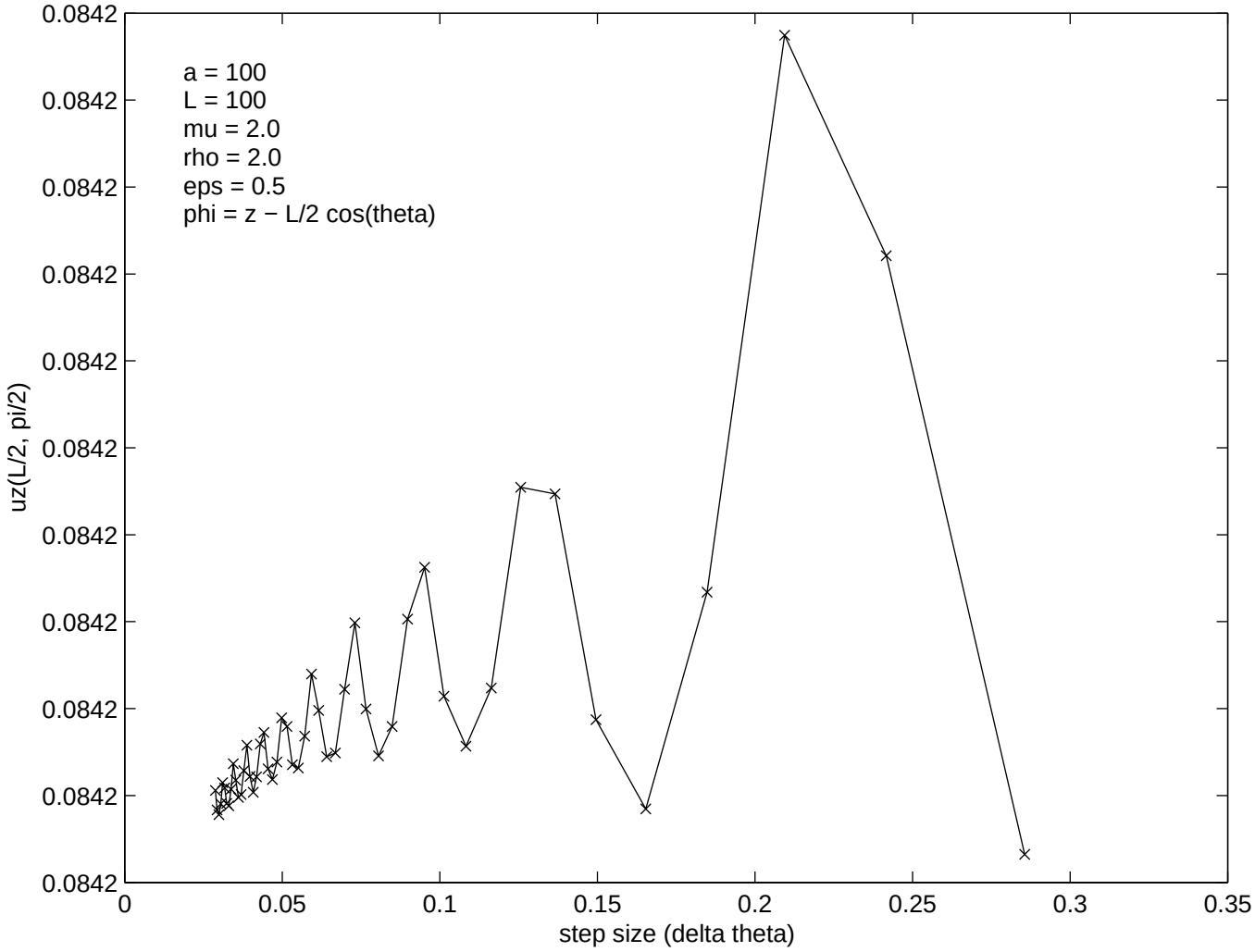

Figure 1: Graph showing velocity away from interface against step size for example data

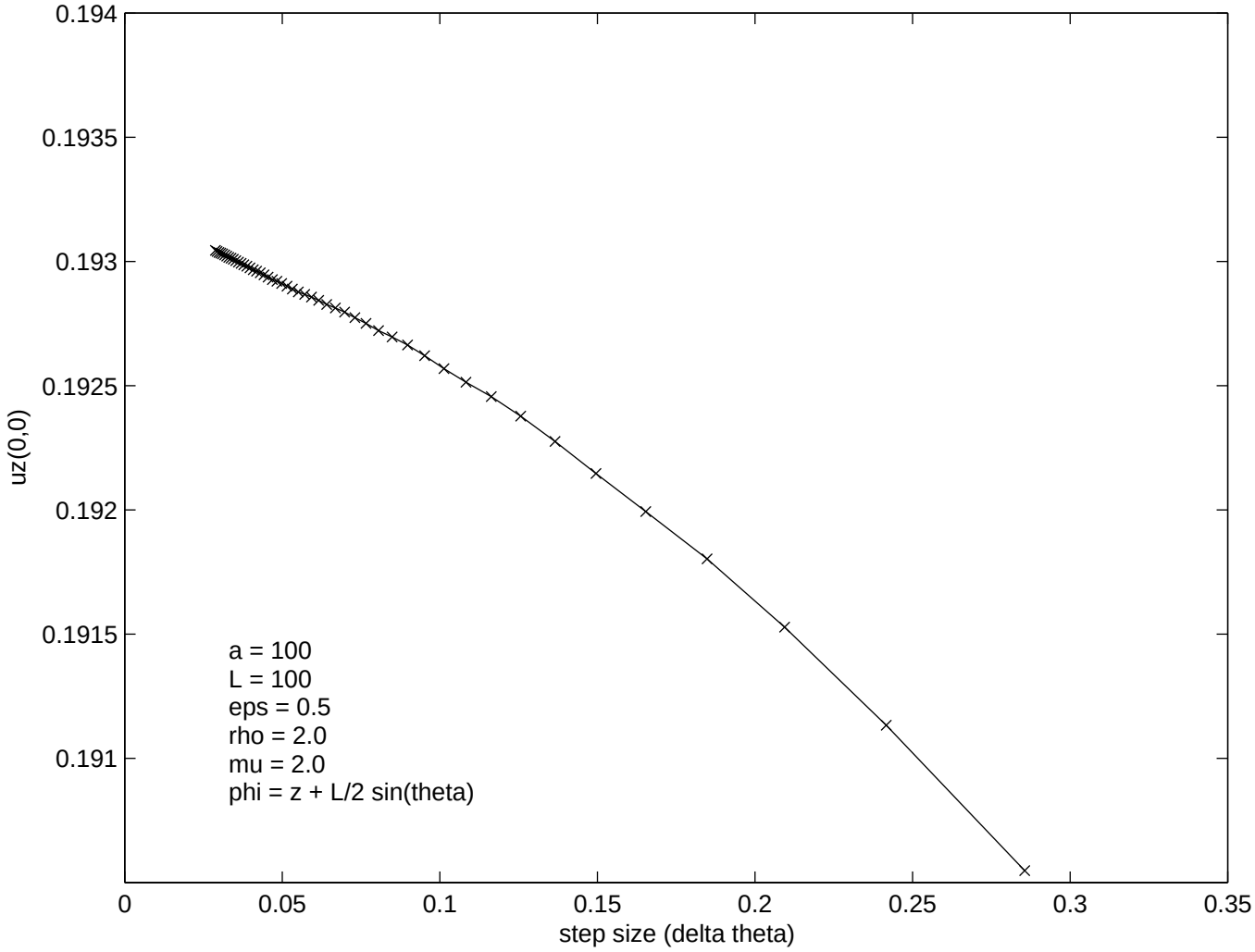

Figure 2: Graph showing velocity on interface against step size for example data

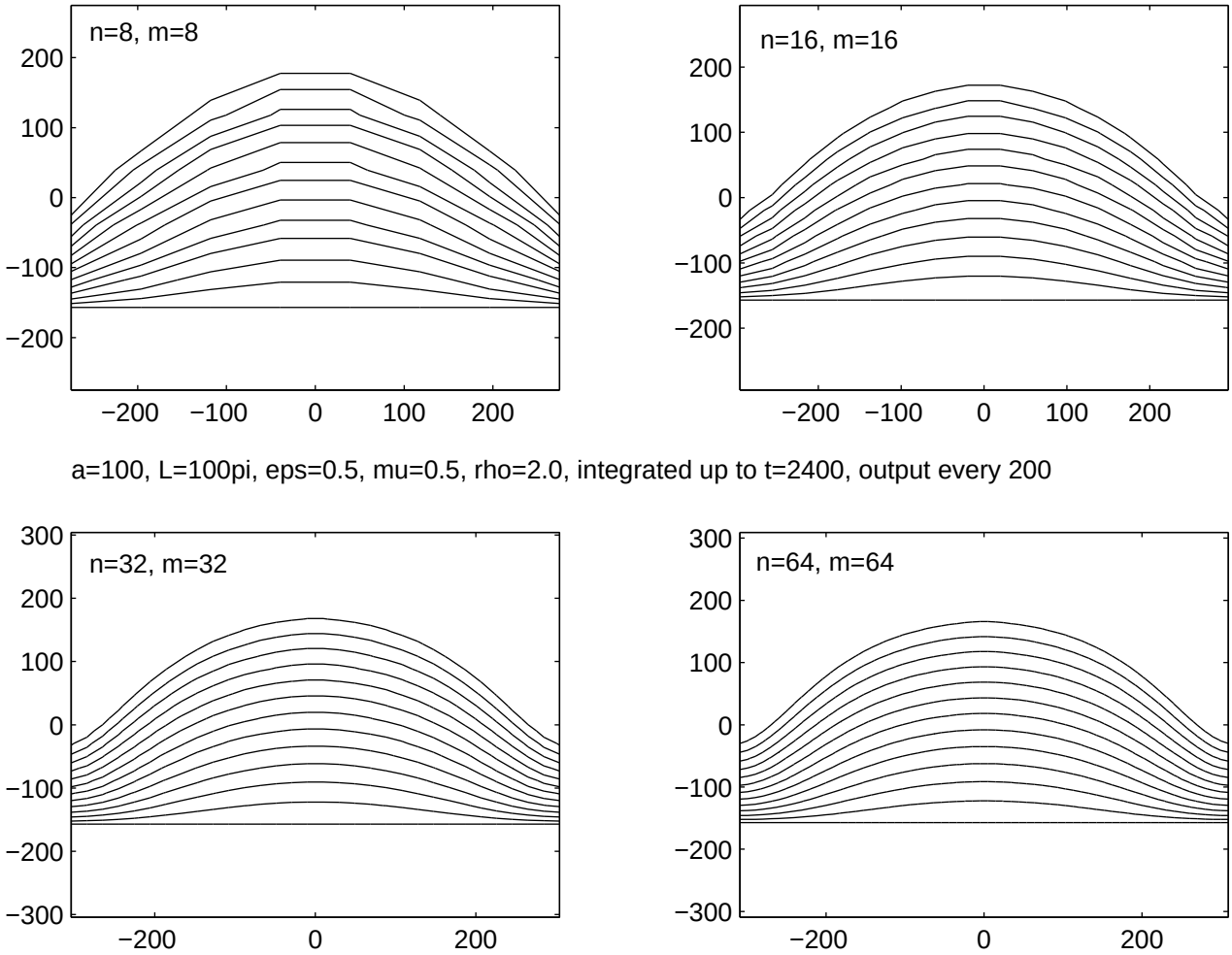

Figure 3: Graph showing an example run for different step sizes, demonstrating convergence ($a\theta$ on the horizontal axes, z on the vertical axes.)

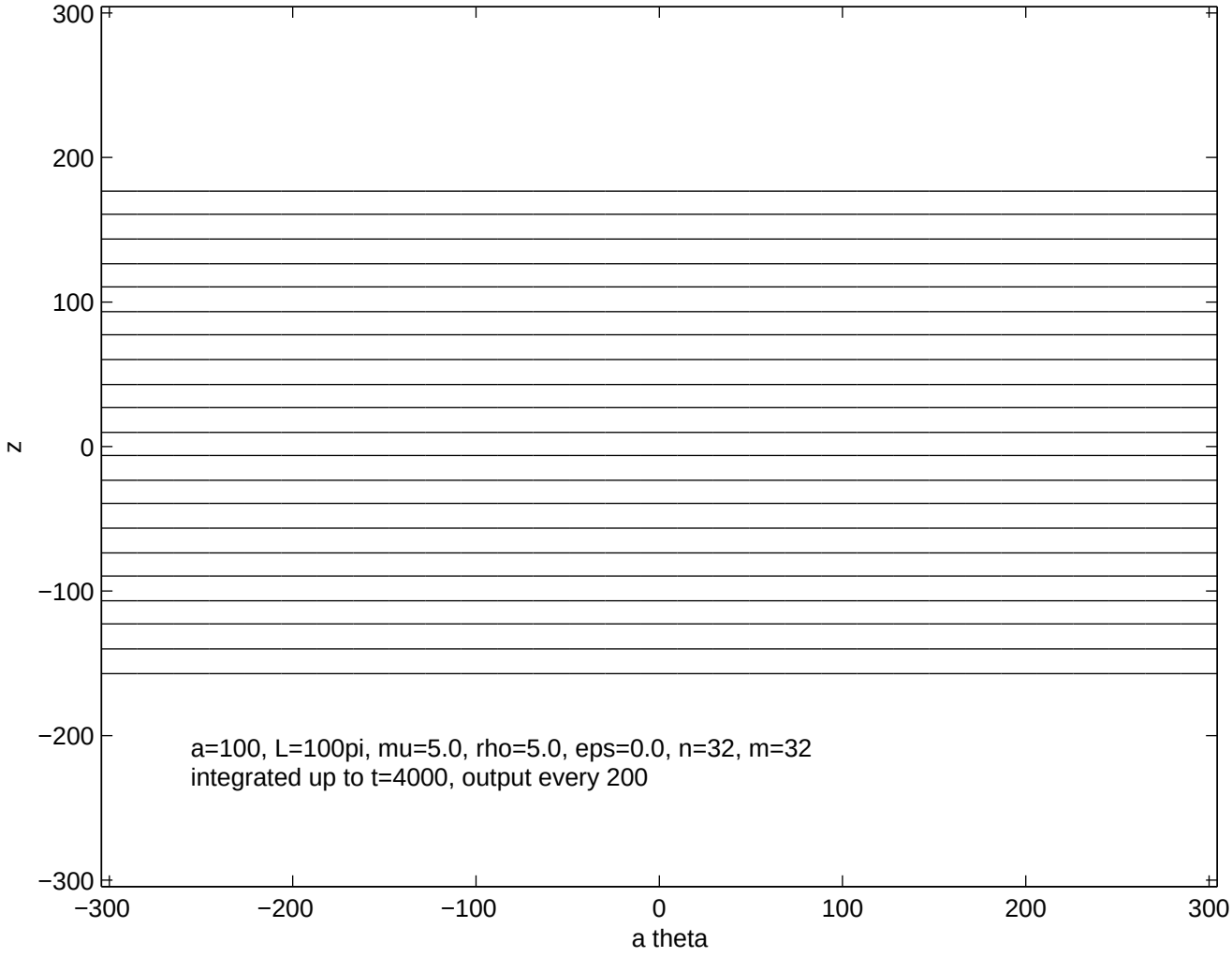

Figure 4: Graph showing simple advection for the case of zero eccentricity

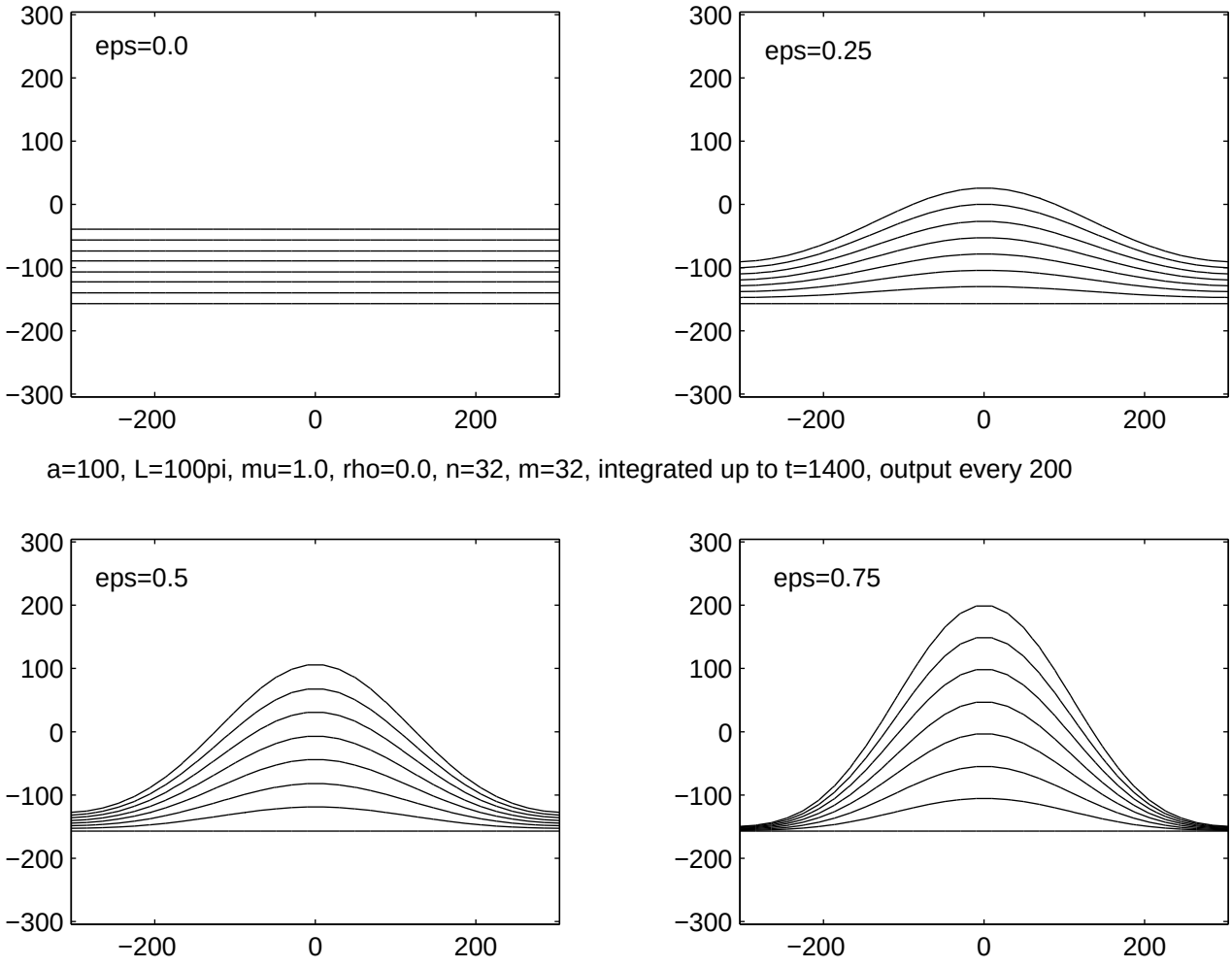

Figure 5: Graph showing the effect of eccentricity.

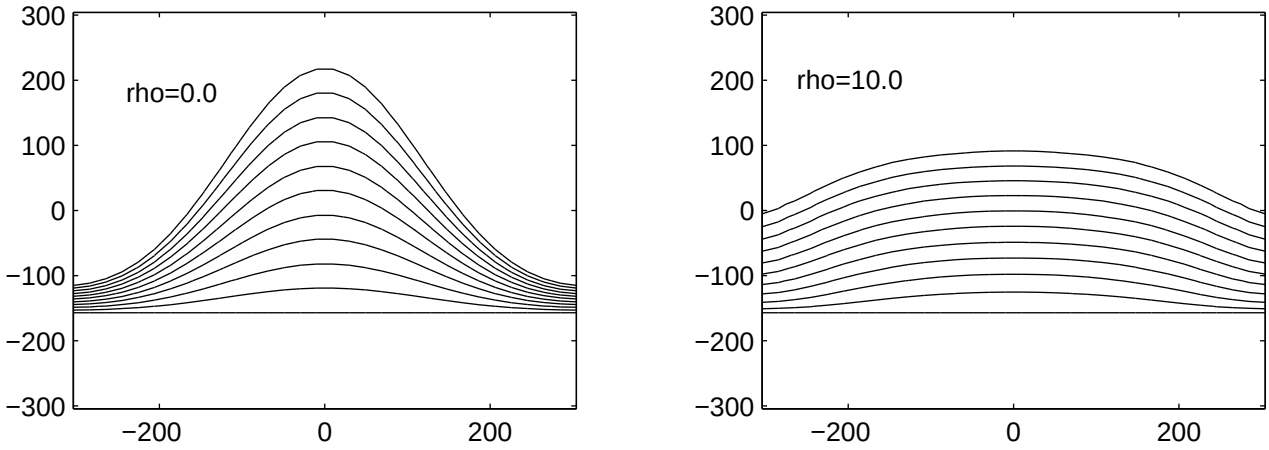

a=100, L=100pi, mu=1.0, eps=0.5, n=32, m=32, integrated up to t=2000, output every 200.

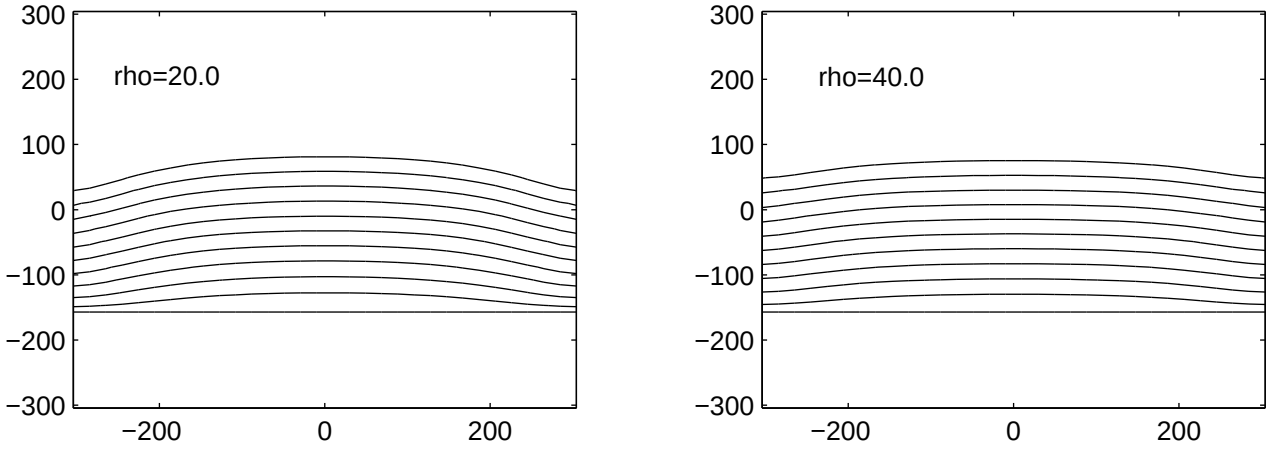

Figure 6: Graph showing the effect of density difference, with the cement more dense

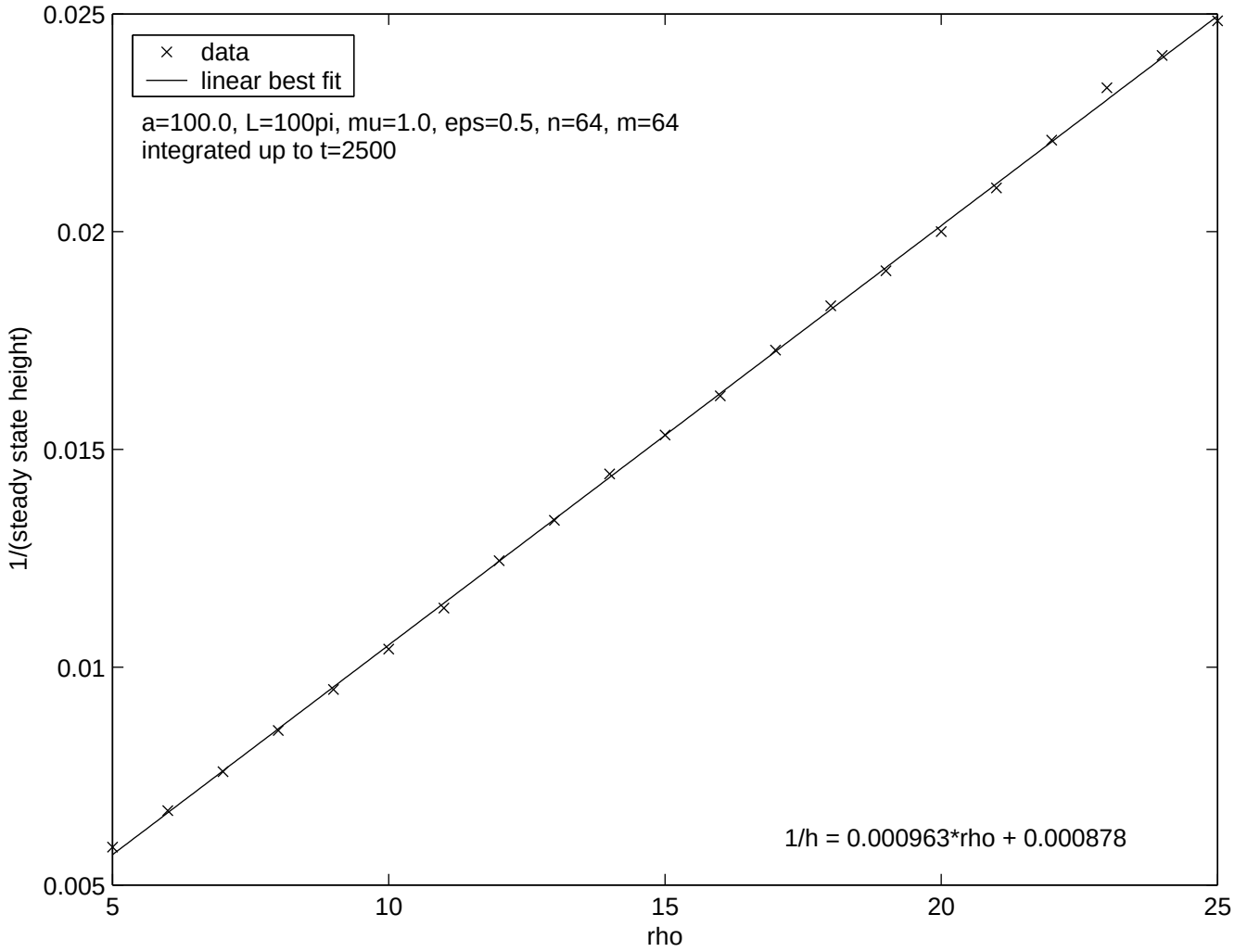

Figure 7: Graph showing the linear variation between density difference and the reciprocal of the steady state height

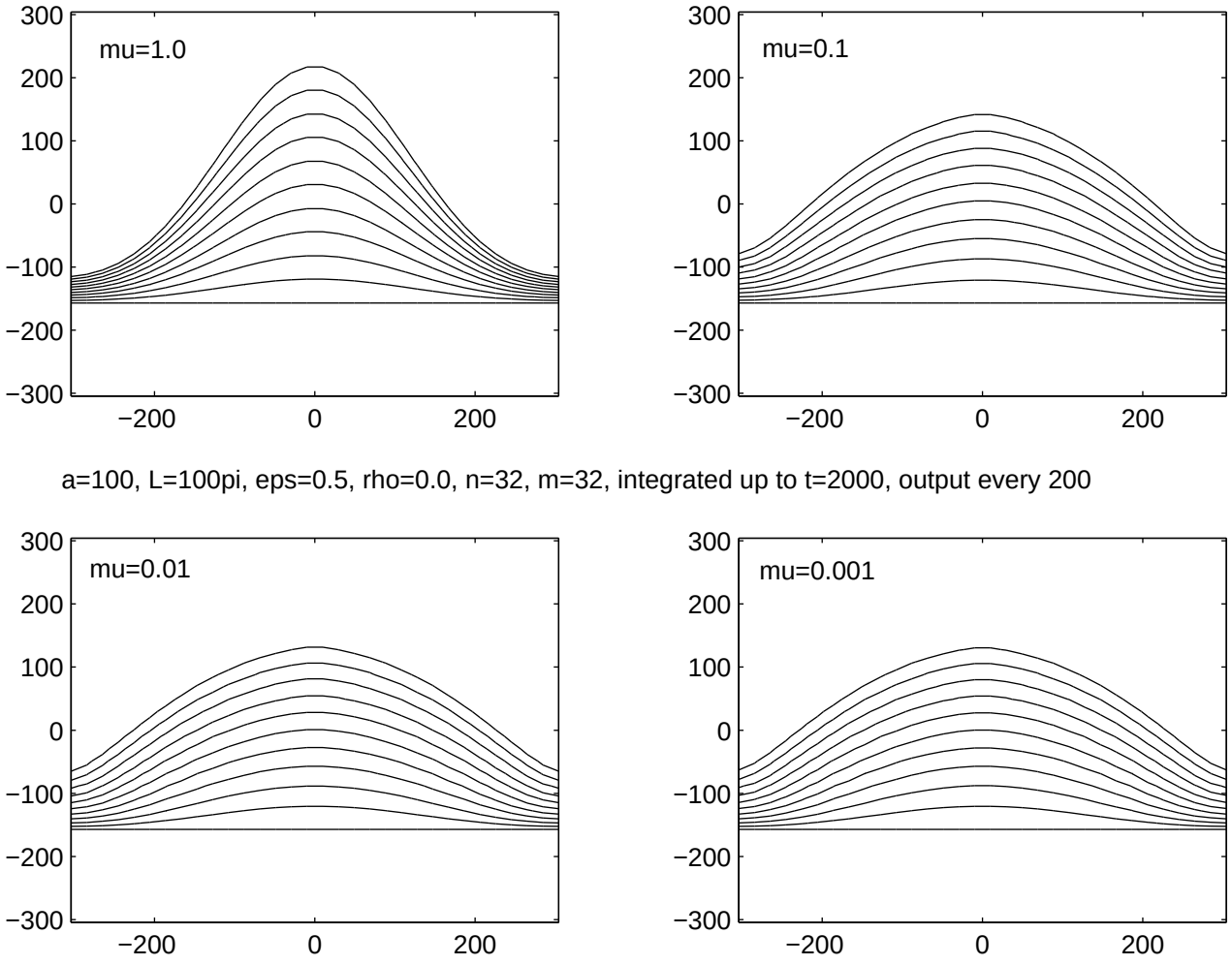

Figure 8: Graph showing the effect of viscosity difference, with the cement more viscous

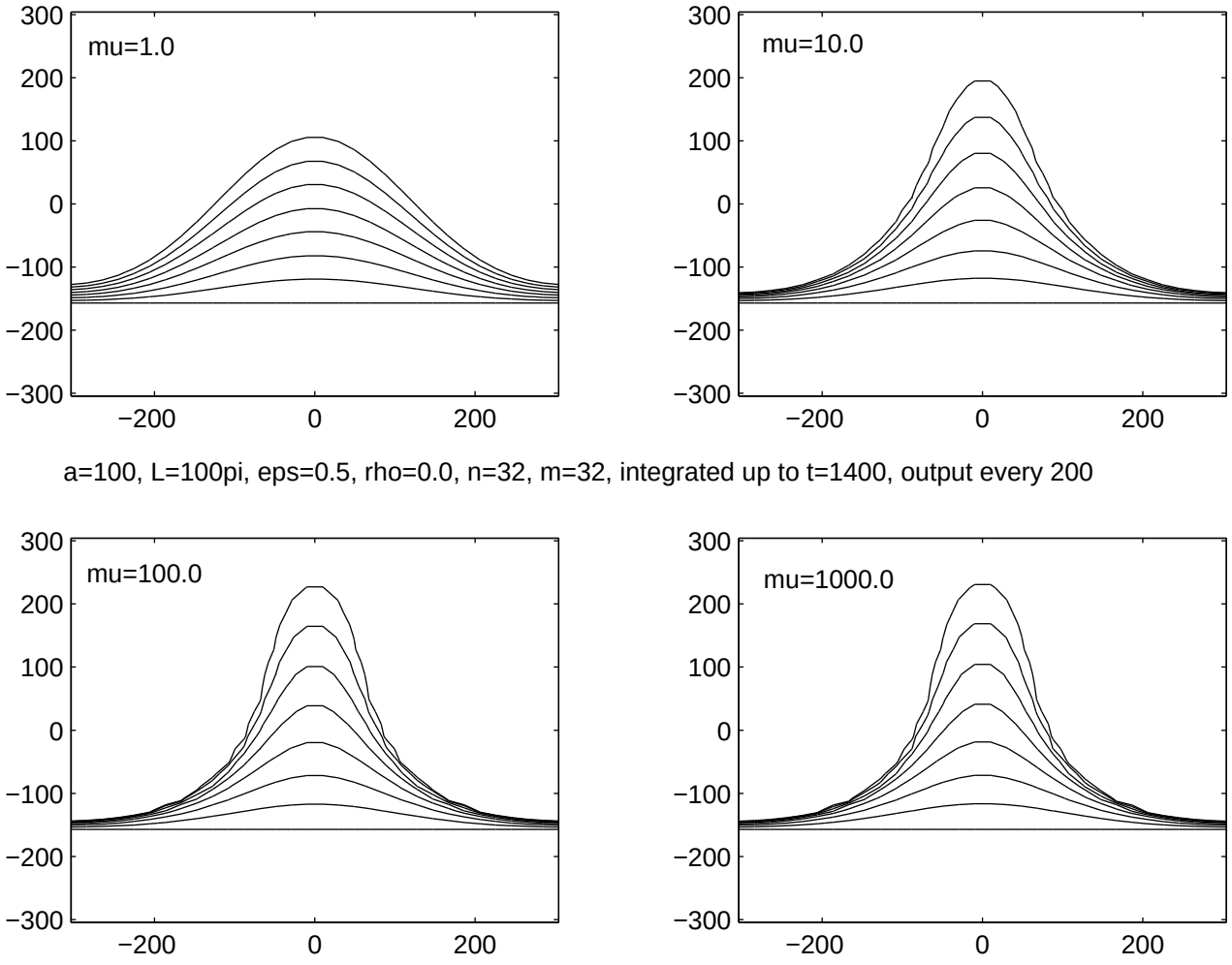

Figure 9: Graph showing the effect of viscosity difference, with the cement less viscous

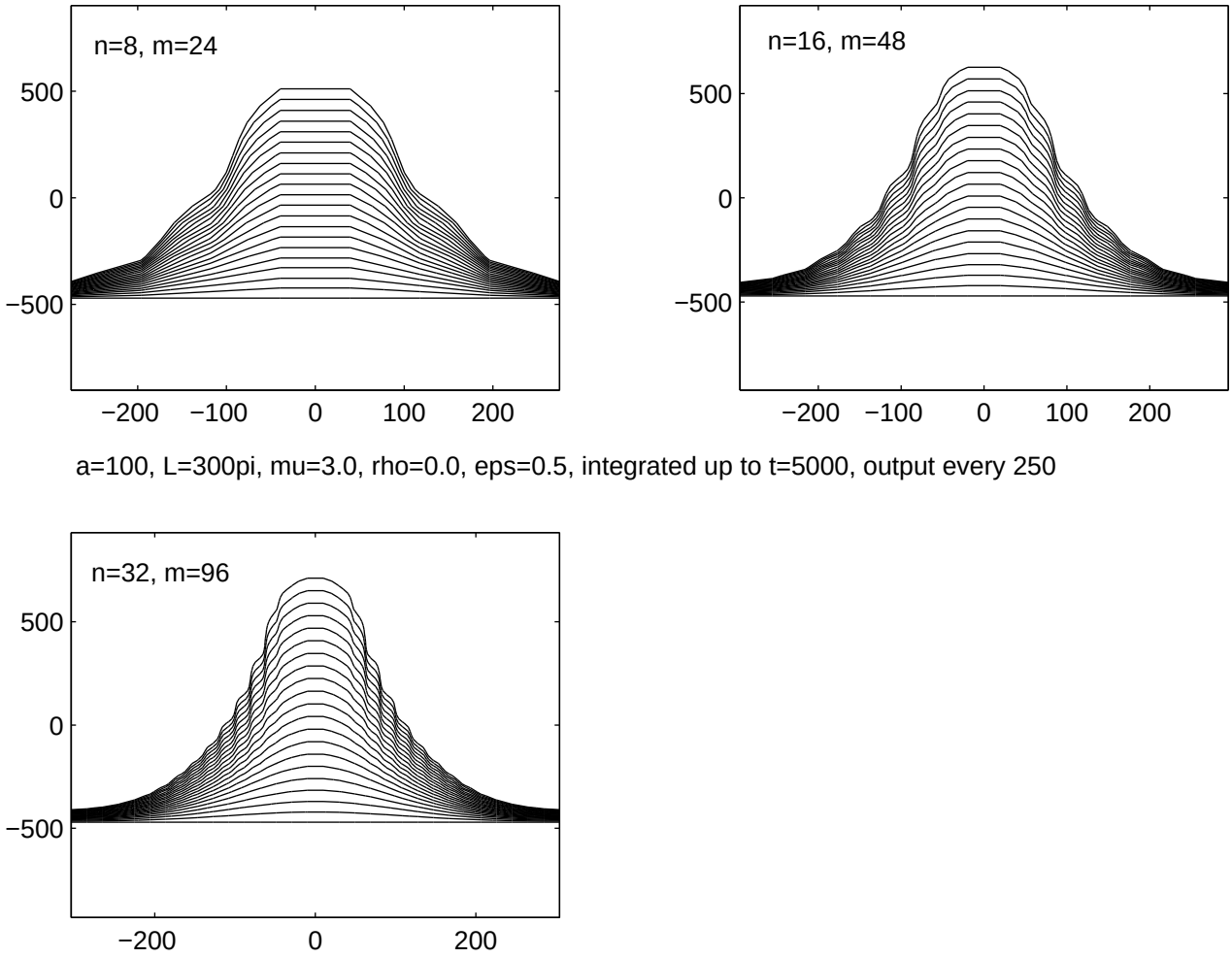

Figure 10: Graph showing the dependence of the viscous instability on step size